University of Glasgow

Peloni, A. , McInnes, C. R. and Ceriotti, M. (2018) Osculating Keplerian elements for highly non-Keplerian orbits. *Journal of Guidance, Control, and Dynamics*, 41(11), pp. 2489-2498. (doi:10.2514/1.G002867)

This is the author's final accepted version.

There may be differences between this version and the published version. You are advised to consult the publisher's version if you wish to cite from it.

http://eprints.gla.ac.uk/163595/

Deposited on: 08 June 2018

Enlighten – Research publications by members of the University of Glasgow
http://eprints.gla.ac.uk

Osculating Keplerian Elements for Highly Non-Keplerian Orbits

Alessandro Peloni,* Colin R. McInnes,† and Matteo Ceriotti‡

University of Glasgow, Glasgow G12 8QQ, United Kingdom

I. Introduction

Celestial mechanics conventionally deals with Keplerian orbits, treating any non-Keplerian effect as a perturbation to the classical Keplerian orbit. However, a non-Keplerian orbit is defined as an orbit in which a perturbative or propulsive acceleration acts in addition to the gravitational attraction of the primary body. Following the definition given in McKay et al. [1], a highly non-Keplerian orbit (NKO) is characterized by the magnitude of the average propulsive acceleration over one orbit $\|\boldsymbol{a}_{av}\|$ equal or greater than the sum of gravitational and centripetal force experienced by the orbiting body $\|\nabla U\|$. That is, introducing a parameter λ to represent this ratio, a NKO is characterized by $\lambda = \|\boldsymbol{a}_{av}\| / \|\nabla U\| \geq 1$.

New families of NKOs can be generated using continuous low-thrust propulsion [1-4]. These include orbits displaced above/below the orbit plane of a conventional Keplerian orbit using out-of-plane thrust, or inside/outside a Keplerian orbit using radial thrust. For a given NKO radius, displacement distance and orbit period the required thrust magnitude and direction can be determined analytically [2]. In addition, the linear stability properties of the families of highly non-Keplerian orbits can be determined and it can be shown that while unstable families of orbits exist they are in principle controllable using feedback to the thrust direction and/or modulation of the thrust

---

* Research Assistant, School of Engineering, James Watt (South) Building; alessandro.peloni@gmail.com.

† Professor, School of Engineering, James Watt (South) Building; Colin.McInnes@glasgow.ac.uk.

‡ Lecturer, School of Engineering, James Watt (South) Building; Matteo.Ceriotti@glasgow.ac.uk. Member AIAA.

The content of this paper was presented at the 27th AAS/AIAA Space Flight Mechanics Meeting held in San Antonio, TX, USA on February, 5-9 2017. AAS Paper 17-278.

magnitude [3]. Moreover, the nonlinear stability properties of NKOs have also been investigated, and the sufficient and necessary conditions for stability of motion near the equilibria have been obtained [5].

In addition, by terminating the low-thrust perturbation, a Keplerian orbit will result allowing Keplerian and highly non-Keplerian orbits to be patched together to generate rich and complex families of composite orbits that have yet to be fully explored [6]. Potential applications of NKOs include orbits displaced above/below the geostationary ring to increase the number of available slots for communications platforms [4] and on-orbit inspection by formation-flying above/below or inside/outside the orbit of a target spacecraft [7]. For example, a displacement distance of 35 km north/south of the geostationary ring allows a platform on a displaced highly non-Keplerian orbit to sit above/below the standard 70 km station-keeping box of a conventional geostationary platform. Such an orbit would require a thrust of 200 mN for a 1000 kg spacecraft, which is achievable with a single QinetiQ T6+ thruster [4].

To date, several studies have been undertaken to investigate families of NKOs. As demonstrated in the survey presented by McKay et al. [1], the problem has been tackled by considering different propulsion technologies and different dynamical models. Different mission applications are also outlined for NKOs, such as telecommunications [7], Earth or Sun observation [8, 9], planetary science [10] and climate engineering [11]. The coupling between orbit and attitude dynamics has been investigated for both a solar sail [12] and an electric sail [13] in a NKO displaced above the ecliptic plane. The use of out-of-plane displaced NKOs is shown advantageous also for towing near-Earth asteroids [14]. Note that all the cited studies deal with a subset of NKOs, which are those displaced above/below the plane of the corresponding conventional Keplerian orbit. For this reason, the term “highly non-Keplerian orbit” coined by McKay et al. [1] is preferred in this note against the term “displaced non-Keplerian orbit”.

As discussed above, all prior studies on highly non-Keplerian orbits have focused on orbit and mission-design. A key open issue in the analysis of the families of NKOs is the generation of a mapping from the NKO geometry to a corresponding set of osculating orbital elements. This is of importance both to support the future operational use of NKOs and to understand the signature of a highly non-Keplerian orbit. Since families of NKOs are generated using a strong, continuous perturbation, their osculating orbital elements will be time-varying, although still periodic. Similarly, the inverse problem is also of importance to deduce the NKO geometry from observations of orbital elements. Once these elements are known, the thrust-induced acceleration magnitude and direction required for the highly non-Keplerian orbit can also be determined.

To pursue these questions, the key objectives of this note are to: a) map the properties of families of NKOs onto the classical orbital elements; b) generate an inverse mapping from orbital elements to the properties of the NKOs; and c) determine the key signatures of NKOs. These objectives represent a largely unexplored aspect of the dynamics of families of NKOs and offer a route towards their future operational use.

II. Highly Non-Keplerian Orbits

Circular highly non-Keplerian orbits can be obtained considering the dynamics of a low-thrust propelled spacecraft in a rotating reference frame [2]. The free parameters of the problem are the angular velocity of rotation of the reference frame ϖ, the out-of-plane displacement z, the radius of the orbit ρ, the inclination of the orbit j, and the right ascension of the ascending node (RAAN) of the orbit ξ (Fig. 1). Note that the symbols $\{j,\xi\}$ have been used for the description of the NKO elements inclination and RAAN because these elements should not be confused with the osculating counterparts. It can be demonstrated that stationary solutions of the equations of motion in this rotating reference frame correspond to periodic, displaced, circular orbits with the orbital plane parallel to the plane defined by j and ξ when viewed from an inertial reference frame (the Earth-Centered Inertial (ECI) frame $\left\{\hat{\boldsymbol{X}},\hat{\boldsymbol{Y}},\hat{\boldsymbol{Z}}\right\}$ is considered in this note). The acceleration needed to generate such stationary solutions can be derived in a closed, analytical form [2]. The thrust vector lies in the plane spanned by the radius vector and the orbital angular momentum unit vector $\hat{\boldsymbol{h}}$, as shown in Fig. 1. Following [2], it can be shown that the propulsive acceleration vector can be described, as a function of the NKO elements $\boldsymbol{x}_{NKO}=\left[z,\rho,\varpi,j,\xi\right]^T$, by its magnitude $\|\boldsymbol{a}\|$ and pitch angle α, as follows.

$$\begin{cases} \left\|\boldsymbol{a}\left(z,\rho,\varpi,j,\xi\right)\right\| = \sqrt{\rho^2\left(\varpi^2-\varpi_*^2\right)^2+z^2\varpi_*^4} \\ \tan\alpha\left(z,\rho,\varpi,j,\xi\right) = \dfrac{\rho}{z}\left[1-\left(\dfrac{\varpi}{\varpi_*}\right)^2\right] \end{cases} \tag{1}$$

The term $\varpi_*=\sqrt{\mu/r^3}$ in Eq. (1) is the orbital angular velocity of a Keplerian orbit of radius $r=\sqrt{\rho^2+z^2}$. Viewed from an inertial reference frame, the orbits generated by the acceleration described in Eq. (1) correspond to circular orbits displaced above the central body and with an orbit plane rotated following the rotations

$R_3(\xi) \to R_1(j)$. The angular velocity of the rotation of the reference frame ϖ corresponds to the angular velocity of the circular orbit viewed from an inertial reference frame.

The acceleration defined in Eq. (1) is that required to generate stationary solutions in the rotating reference frame (i.e. $\|\boldsymbol{a}\| = \|\nabla U\|$). Therefore, such solutions are characterized by $\lambda = 1$ and so are defined as highly non-Keplerian orbits.

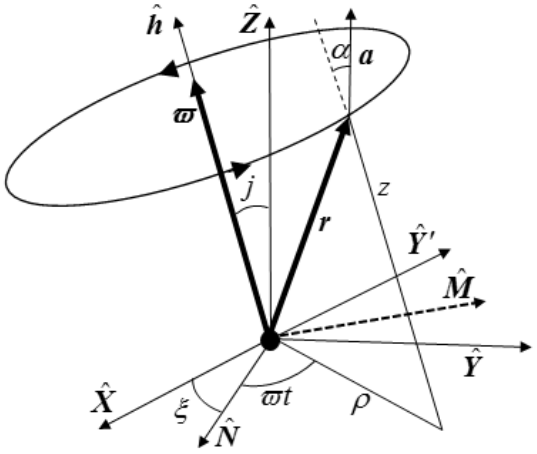

Fig. 1 Schematic out-of-plane displaced highly non-Keplerian orbit with thrust-induced acceleration.

Three families of NKOs can be defined based on the value of the angular velocity of the rotating reference frame [2]. Type 1 NKOs are defined as those orbits with the minimum required acceleration. From Eq. (1), the requirement of minimum acceleration leads to an angular velocity of the rotating reference frame for Type 1 NKOs defined as shown in Eq. (2). A second family of NKOs is characterized by orbits synchronous with a body on a circular Keplerian orbit in the $z = 0$ plane with the same orbit radius. Lastly, a third family of NKOs is defined by setting the orbital period to a fixed value. The angular velocities that characterize the three families of NKOs are shown in Eq. (2).

$$\varpi_{\text{Type 1}} = \sqrt{\mu / r^3}, \quad \varpi_{\text{Type 2}} = \sqrt{\mu / \rho^3}, \quad \varpi_{\text{Type 3}} = \varpi_0 \tag{2}$$

Note that Type 1 and Type 2 NKOs are, by definition, orbits displaced out-of-plane respect to the corresponding Keplerian orbits. In fact, one fundamental characteristic of both Type 1 and Type 2 NKOs is that the primary body is not contained within the orbital plane. On the contrary, Type 3 NKOs can be characterized by either an out-of-plane or an in-plane displacement with respect to the corresponding Keplerian orbits.

III. Forward Map: Highly Non-Keplerian Orbit to Osculating Orbital Elements

In this section, the mappings between NKO elements and the osculating orbit are derived in closed, analytical form for the direct problem. Two sets of orbital elements are chosen to describe the osculating Keplerian orbit: a) classical Keplerian elements (KEP) $\boldsymbol{x}_{KEP} = \left[a, e, i, \Omega, \omega, \vartheta\right]^T$, and b) modified equinoctial elements (MEE) $\boldsymbol{x}_{MEE} = \left[p, f, g, h, k, L\right]^T$.

Starting from the NKO elements $\boldsymbol{x}_{NKO} = \left[z, \rho, \varpi, j, \xi\right]^T$, the Cartesian position vector $\boldsymbol{r}$ and velocity vector $\boldsymbol{v}$ are given by

$$\boldsymbol{r} = \begin{bmatrix} \rho\left(\cos\xi\cos\left(\varpi t\right) - \cos j \sin\xi \sin\left(\varpi t\right)\right) + z \sin j \sin\xi \\ \rho\left(\sin\xi\cos\left(\varpi t\right) + \cos j \cos\xi \sin\left(\varpi t\right)\right) - z \sin j \cos\xi \\ \rho \sin j \sin\left(\varpi t\right) + z\cos j \end{bmatrix} \tag{3}$$

$$\boldsymbol{v} = \varpi\rho \begin{bmatrix} -\cos\xi\sin\left(\varpi t\right) - \cos j \sin\xi\cos\left(\varpi t\right) \\ -\sin\xi\sin\left(\varpi t\right) + \cos j \cos\xi\cos\left(\varpi t\right) \\ \sin j \cos\left(\varpi t\right) \end{bmatrix} \tag{4}$$

From the Cartesian position and velocity vectors described in Eqs. (3) - (4), the forward maps are derived in the following sections for each one of the osculating orbital elements considered.

Moreover, a sensitivity analysis has been performed to study the behavior of the mappings in presence of errors in the NKO elements. Both analytical and numerical sensitivity analyses have been carried out to confirm the results found. The analytical sensitivity analysis is centered on the computation of the Jacobian $\mathbf{J}$ of the mapping.

A. NKO to Osculating KEP

From Eqs. (3) - (4), the NKO to osculating KEP map can be derived following the conversion from Cartesian position and velocity to KEP, as described in [15]. The resulting map is shown in Eq. (5).*

---

* For the full derivation of this and the following maps, the interested reader is referred to: Peloni, A., McInnes, C. R. and Ceriotti, M., "Osculating Keplerian Elements for Highly Non-Keplerian Orbits", University of Glasgow - Air Force Office of Scientific Research, Report No. AD1031622, 2017, 27 March 2017, pp. 99, http://www.dtic.mil/docs/citations/AD1031622 [retrieved 06 February 2018].

The first important characteristics of the osculating Keplerian orbits that describe an NKO have already been shown in the forward map. In fact, from the formulation of the true anomaly in Eq. (5), it can be noted that a spacecraft on a NKO is always either at the apocenter or pericenter of the osculating Keplerian orbit. Moreover, it is important to underline that $\Omega = 0$ is arbitrarily chosen in the case of a planar NKO.

It is interesting to study the case for which the orbital plane of the NKO is parallel to the $\hat{\boldsymbol{X}} - \hat{\boldsymbol{Y}}$ plane. That is, $j = \xi = 0$. In the reminder of this note, this case will be referred to as the "vertical-displacement model" to highlight the fact that there are no changes in the orientation of the orbital plane with respect to the $\hat{\boldsymbol{X}} - \hat{\boldsymbol{Y}}$ plane.

Considering the vertical-displacement model, the forward map shown in Eq. (5) can be rewritten, after algebraic manipulations, as shown in Eq. (7).

It is worth noting that the case $\left(z \neq 0 \wedge \mu = \varpi^2 \rho^2 \sqrt{\rho^2 + z^2}\right)$ is not considered in the formulation of ω and ϑ in Eq. (7). However, this case corresponds to an osculating circular orbit, which is not possible for the types of NKOs considered within this study. Equation (7) shows that $\omega = 0$ only if $z = 0 \wedge \mu = \varpi^2 \rho^3$, which is the condition for a Keplerian orbit. Lastly, it can be noted that the osculating argument of pericenter is always constant for an out-of-plane-displaced NKO.

For the sensitivity analysis, an analytical study can be carried out only on those elements characterized by a continuous function (i.e. semi-major axis, eccentricity, and inclination). Only a numerical sensitivity analysis can be carried out on the last three elements of the map. The parameters used to test the sensitivity of the mapping to uncertainties in an NKO element x_i depend on the classical Keplerian element and are (Eq. (8)): a) relative error of the semi-major axis; b) absolute error of the eccentricity; c) normalized error of the general angles $\psi = \{i, \Omega, \omega, \vartheta\}$.

B. NKO to Osculating MEE

To have a mapping with no singularities, a map from Cartesian position and velocity to osculating modified equinoctial elements is derived. In fact, MEE have been introduced to avoid singularities occurring in Keplerian orbits in the case of planar and/or circular orbits [16]. Starting from the expressions of the Cartesian position and velocity vectors (Eqs. (3) - (4)) and the analytical mapping of the osculating KEP shown in Eq. (5), the mapping from NKO elements to osculating MEE is shown in Eq. (9), in which Ω^* and γ are defined in Eq. (6).

As for the case of the use of classical Keplerian elements, also here the map is characterized by a piecewise formulation for three elements. Nevertheless, if the vertical-displacement model is considered, the map shown in Eq. (9) can be rewritten, after some algebraic manipulation, as shown in Eq. (10).

$$
\begin{aligned}
a &= \frac{\mu\sqrt{\rho^2+z^2}}{2\mu-\varpi^2\rho^2\sqrt{\rho^2+z^2}} \qquad e = \frac{\left|\mu-\varpi^2\rho^2\sqrt{\rho^2+z^2}\right|}{\mu} \\
i &= \arccos\left(\frac{\rho\cos j - z\sin j\sin(\varpi t)}{\sqrt{\rho^2+z^2}}\right) \quad \Omega = \begin{cases} 0 & \text{if } z=0 \wedge j=0 \\ \Omega^* & \text{otherwise} \end{cases} \\
\omega &= \begin{cases} 0 & \text{if } \mu = \varpi^2\rho^2\sqrt{\rho^2+z^2} \\ \varpi t & \text{if } j=0 \wedge z=0 \wedge \mu < \varpi^2\rho^3 \\ \pi+\varpi t & \text{if } j=0 \wedge z=0 \wedge \mu > \varpi^2\rho^3 \\ \omega^* & \text{if } \left(\mu-\varpi^2\rho^2\sqrt{\rho^2+z^2}\right)\left(z\cos j+\rho\sin j\sin(\varpi t)\right)\le 0 \\ 2\pi-\omega^* & \text{otherwise} \end{cases} \\
\vartheta &= \begin{cases} \varpi t & \text{if } z=0 \wedge \mu = \varpi^2\rho^3 \\ 0 & \text{if } \mu < \varpi^2\rho^2\sqrt{\rho^2+z^2} \\ \pi & \text{if } \mu > \varpi^2\rho^2\sqrt{\rho^2+z^2} \end{cases}
\end{aligned}
\tag{5}
$$

in which

$$
\begin{aligned}
\Omega^* &= \begin{cases} \arccos\left(N_x/N\right) & \text{if } N_y \ge 0 \\ 2\pi-\arccos\left(N_x/N\right) & \text{otherwise} \end{cases} \\
N &= \sqrt{z^2\cos^2(\varpi t)+\left(\rho\sin j+z\cos j\sin(\varpi t)\right)^2} \\
N_x &= \rho\sin j\cos\xi + z\left(\cos j\cos\xi\sin(\varpi t)+\sin\xi\cos(\varpi t)\right) \\
N_y &= \rho\sin j\sin\xi + z\left(\cos j\sin\xi\sin(\varpi t)-\cos\xi\cos(\varpi t)\right) \\
\omega^* &= \arccos\left(-\gamma\,\mathrm{sgn}\left(\mu-\varpi^2\rho^2\sqrt{\rho^2+z^2}\right)\right) \\
\gamma &= \frac{\sin j\cos(\varpi t)\sqrt{\rho^2+z^2}}{\sqrt{z^2\cos^2(\varpi t)+\left(\rho\sin j+z\cos j\sin(\varpi t)\right)^2}}
\end{aligned}
\tag{6}
$$

$$a = \frac{\mu\sqrt{\rho^2+z^2}}{2\mu-\varpi^2\rho^2\sqrt{\rho^2+z^2}} \quad e = \frac{\left|\mu-\varpi^2\rho^2\sqrt{\rho^2+z^2}\right|}{\mu}$$

$$i = \arccos\left(\frac{\rho}{\sqrt{\rho^2+z^2}}\right)$$

$$\Omega = \begin{cases} 0 & \text{if } z = 0 \\ \arccos\left(\sin\left(\varpi t\right)\operatorname{sgn}\left(z\right)\right) & \text{if } \left(\cos\left(\varpi t\right) \le 0 \wedge z > 0\right) \vee \left(\cos\left(\varpi t\right) \ge 0 \wedge z < 0\right) \\ 2\pi - \arccos\left(\sin\left(\varpi t\right)\operatorname{sgn}\left(z\right)\right) & \text{otherwise} \end{cases}$$

$$\omega = \begin{cases} 0 & \text{if } z = 0 \wedge \mu = \varpi^2\rho^3 \\ \varpi t & \text{if } z = 0 \wedge \mu < \varpi^2\rho^3 \\ \pi + \varpi t & \text{if } z = 0 \wedge \mu > \varpi^2\rho^3 \\ \pi/2 & \text{if } \left(z > 0 \wedge \mu < \varpi^2\rho^2\sqrt{\rho^2+z^2}\right) \vee \left(z < 0 \wedge \mu > \varpi^2\rho^2\sqrt{\rho^2+z^2}\right) \\ 3\pi/2 & \text{if } \left(z > 0 \wedge \mu > \varpi^2\rho^2\sqrt{\rho^2+z^2}\right) \vee \left(z < 0 \wedge \mu < \varpi^2\rho^2\sqrt{\rho^2+z^2}\right) \end{cases}$$

$$\vartheta = \begin{cases} \varpi t & \text{if } z = 0 \wedge \mu = \varpi^2\rho^3 \\ 0 & \text{if } \mu < \varpi^2\rho^2\sqrt{\rho^2+z^2} \\ \pi & \text{if } \mu > \varpi^2\rho^2\sqrt{\rho^2+z^2} \end{cases} \tag{7}$$

$$\varepsilon_{a,x_i} := \frac{\left|J_{a,x_i}\cdot\delta x_i\right|}{a}, \quad \varepsilon_{e,x_i} := \left|J_{e,x_i}\cdot\delta x_i\right|, \quad \varepsilon_{\psi,x_i} := \frac{\operatorname{mod}\left(J_{\psi,x_i}\cdot\delta x_i,\pi\right)}{\pi} \tag{8}$$

$$p = \frac{\varpi^2\rho^2\left(\rho^2+z^2\right)}{\mu}$$

$$f = \frac{\varpi^2\rho^2\sqrt{\rho^2+z^2}-\mu}{\mu}\cdot\begin{cases} \cos\left(\varpi t\right) & \text{if } z = 0 \wedge j = 0 \\ \cos\left(\Omega^* + \arccos\left(\gamma\right)\right) & \text{if } z\cos j + \rho\sin j\sin\left(\varpi t\right) \ge 0 \\ \cos\left(\Omega^* - \arccos\left(\gamma\right)\right) & \text{if } z\cos j + \rho\sin j\sin\left(\varpi t\right) < 0 \end{cases}$$

$$g = \frac{\varpi^2\rho^2\sqrt{\rho^2+z^2}-\mu}{\mu}\cdot\begin{cases} \sin\left(\varpi t\right) & \text{if } z = 0 \wedge j = 0 \\ \sin\left(\Omega^* + \arccos\left(\gamma\right)\right) & \text{if } z\cos j + \rho\sin j\sin\left(\varpi t\right) \ge 0 \\ \sin\left(\Omega^* - \arccos\left(\gamma\right)\right) & \text{if } z\cos j + \rho\sin j\sin\left(\varpi t\right) < 0 \end{cases}$$

$$h = \sqrt{\frac{\sqrt{\rho^2+z^2}-\left(\rho\cos j - z\sin j\sin\left(\varpi t\right)\right)}{\sqrt{\rho^2+z^2}+\left(\rho\cos j - z\sin j\sin\left(\varpi t\right)\right)}}\cdot\frac{\rho\sin j\cos\xi + z\left(\cos j\cos\xi\sin\left(\varpi t\right)+\sin\xi\cos\left(\varpi t\right)\right)}{\sqrt{z^2\cos^2\left(\varpi t\right)+\left(\rho\sin j + z\cos j\sin\left(\varpi t\right)\right)^2}}$$

$$k = \sqrt{\frac{\sqrt{\rho^2+z^2}-\left(\rho\cos j - z\sin j\sin\left(\varpi t\right)\right)}{\sqrt{\rho^2+z^2}+\left(\rho\cos j - z\sin j\sin\left(\varpi t\right)\right)}}\cdot\frac{\rho\sin j\sin\xi + z\left(\cos j\sin\xi\sin\left(\varpi t\right)-\cos\xi\cos\left(\varpi t\right)\right)}{\sqrt{z^2\cos^2\left(\varpi t\right)+\left(\rho\sin j + z\cos j\sin\left(\varpi t\right)\right)^2}}$$

$$L = \begin{cases} \varpi t & \text{if } z = 0 \wedge j = 0 \\ \Omega^* + \arccos\left(\gamma\right) & \text{if } z\cos j + \rho\sin j\sin\left(\varpi t\right) \ge 0 \\ \Omega^* - \arccos\left(\gamma\right) & \text{if } z\cos j + \rho\sin j\sin\left(\varpi t\right) < 0 \end{cases} \tag{9}$$

$$
\begin{aligned}
p &= \frac{\varpi^2\rho^2\left(\rho^2+z^2\right)}{\mu} & h &= -\frac{\sin(\varpi t)\left(\rho-\sqrt{\rho^2+z^2}\right)}{z} \\
f &= \frac{\varpi^2\rho^2\sqrt{\rho^2+z^2}-\mu}{\mu}\cos(\varpi t) & k &= \frac{\cos(\varpi t)\left(\rho-\sqrt{\rho^2+z^2}\right)}{z} \\
g &= \frac{\varpi^2\rho^2\sqrt{\rho^2+z^2}-\mu}{\mu}\sin(\varpi t) & L &= \varpi t
\end{aligned}
\tag{10}
$$

It is worth noting that, in Eq. (10), there are no singularities in the formulations of the out-of-plane MEE in the case of zero out-of-plane displacement orbits. It can be seen, in fact, that $\lim_{z\to 0} h = \lim_{z\to 0} k = 0$. Moreover, it is important to note that no assumptions have been made in the derivation of this map. Indeed, the functions that describe the NKO to osculating MEE map are continuous in the whole spectrum of the NKO elements for the vertical-displacement model.

The parameters used to test the sensitivity of the mapping to uncertainties in an NKO element x_i depend on the MEE and are (Eq. (11)): a) relative error of the semi-latus rectum; b) absolute error of the general element $y = \{f, g, h, k\}$; and c) normalized error of the true longitude L.

$$
\varepsilon_{p,x_i} := \frac{\left|J_{p,x_i}\cdot\delta x_i\right|}{p}, \quad \varepsilon_{y,x_i} := \left|J_{y,x_i}\cdot\delta x_i\right|, \quad \varepsilon_{L,x_i} := \frac{\mathrm{mod}\left(J_{L,x_i}\cdot\delta x_i,\pi\right)}{\pi}
\tag{11}
$$

IV. Inverse Map: Osculating Orbital Elements to Highly Non-Keplerian Orbit

After the forward mappings from families of highly non-Keplerian orbits to osculating orbital elements described in the previous section, two different inverse mappings from orbital elements to NKO geometry have been generated for the vertical-displacement model. These mappings have been derived in closed, analytical form. A sensitivity analysis has been performed to understand the impact of uncertainties in the orbital elements on the NKO properties. Only a numerical sensitivity analysis has been carried out by computing the values of the osculating elements from the perturbed input elements and then computing the errors with respect to the nominal values. The parameters used to test the sensitivity of the mapping to uncertainties in the osculating orbital elements are as follows.

- Absolute error of the vertical displacement. The absolute error has been chosen against the relative error because all the NKOs feasible with near-term technology are characterized by small vertical displacements.

- Relative error of the orbit radius. The relative error has been chosen against the absolute error because usually NKOs with small vertical displacements are characterized by large orbit radii.
- Relative error of the orbital angular momentum.

A. Osculating KEP to NKO

Recalling that the radius of the osculating orbit can be expressed, in terms of KEP, as $r = a\left(1-e^2\right)/\left(1+e\cos\vartheta\right)$, the position and velocity vectors in the orbital reference frame $\left\{\hat{\boldsymbol{r}},\hat{\boldsymbol{\vartheta}},\hat{\boldsymbol{h}}\right\}$ are given by

$$\boldsymbol{r}_{orb} = \begin{bmatrix} r\cos\vartheta & r\sin\vartheta & 0 \end{bmatrix}^T, \quad \boldsymbol{v}_{orb} = \begin{bmatrix} \dot{r}\cos\vartheta - r\sin\vartheta\dot{\vartheta} & \dot{r}\sin\vartheta + r\cos\vartheta\dot{\vartheta} & 0 \end{bmatrix}^T \tag{12}$$

in which

$$\begin{cases} \dot{\vartheta} = \dfrac{h}{r^2} = \dfrac{\sqrt{\mu a\left(1-e^2\right)}}{r^2} \\ \dot{r} = \dfrac{\partial}{\partial t}\left(\dfrac{a\left(1-e^2\right)}{1+e\cos\vartheta}\right) = \dfrac{ea\left(1-e^2\right)\sin\vartheta\dot{\vartheta}}{\left(1+e\cos\vartheta\right)^2} = \sqrt{\dfrac{\mu}{a\left(1-e^2\right)}}e\sin\vartheta \end{cases} \tag{13}$$

Therefore, the position and velocity vectors shown in Eq. (12) can be written in the ECI frame by following the rotations $R_3\left(-\omega\right)\rightarrow R_1\left(-i\right)\rightarrow R_3\left(-\Omega\right)$. As such, the map from osculating KEP to NKO elements is summarized as

$$\begin{aligned} z &= \frac{a\left(1-e^2\right)}{1+e\cos\vartheta}\sin i\sin\left(\omega+\vartheta\right) \\ \rho &= \frac{a\left(1-e^2\right)}{2\left(1+e\cos\vartheta\right)}\sqrt{3+\cos\left(2i\right)+2\cos\left(2\left(\omega+\vartheta\right)\right)\sin^2 i} \\ \varpi &= \sqrt{\frac{\mu}{a^3\left(1-e^2\right)^3}}2\left(1+e\cos\vartheta\right)\sqrt{\frac{1+e^2+2e\cos\vartheta}{3+\cos\left(2i\right)+2\cos\left(2\left(\omega+\vartheta\right)\right)\sin^2 i}} \end{aligned} \tag{14}$$

B. Osculating MEE to NKO

From the formulation of Cartesian position and velocity vectors as a function of MEE given in [17], the inverse map from osculating MEE to NKO elements is derived as

$$\begin{aligned} z &= \frac{2r}{s}\left(h\sin L - k\cos L\right) \\ \rho &= \frac{r}{s}\sqrt{1+\left(h^2+k^2\right)^2+2\beta\cos\left(2L\right)+4hk\sin\left(2L\right)} \\ \varpi &= \frac{s}{r}\sqrt{\frac{\mu}{p}}\sqrt{\frac{1+f^2+g^2+2f\cos L+2g\sin L}{1+\left(h^2+k^2\right)^2+2\beta\cos\left(2L\right)+4hk\sin\left(2L\right)}} \end{aligned} \tag{15}$$

in which

$$r = \frac{p}{1 + f\cos L + g\sin L}, \quad s = 1 + h^2 + k^2, \quad \beta = h^2 - k^2 \tag{16}$$

V. Determination of Spacecraft Thrust-Induced Acceleration

The magnitude and direction of the spacecraft thrust-induced acceleration used to generate families of NKOs have been derived by using the inverse mapping from the orbital elements discussed in Sec. IV as inputs for Eq. (1). This analysis links the thrust-induced acceleration to the highly non-Keplerian orbit geometry.

A. Classical Keplerian elements

From Eq. (1) and using the mappings shown in Eq. (14), the magnitude of the thrust-induced acceleration and pitch angle are obtained as

$$\left\| \boldsymbol{a}\left(\boldsymbol{x}_{KEP} \right) \right\| = \frac{\mu\left(1 + e\cos\vartheta\right)}{2a^2\left(1 - e^2\right)^2}\sqrt{A + B} \tag{17}$$

$$\tan\alpha\left(\boldsymbol{x}_{KEP} \right) = \frac{\sqrt{\sigma_1}}{2\sin i\sin\left(\omega + \vartheta\right)}\left[1 - \frac{4\left(1 + e^2 + 2e\cos\vartheta\right)}{\sigma_1\left(1 + e\cos\vartheta\right)} \right] \tag{18}$$

in which

$$\begin{cases} A = 4\left(1 + e\cos\vartheta\right)^2\sin^2 i\sin^2\left(\omega + \vartheta\right) \\ B = \sigma_1\left(1 + e\cos\vartheta - 4\left(1 + e^2 + 2e\cos\vartheta\right)/\sigma_1\right)^2 \\ \sigma_1 = 3 + \cos\left(2i\right) + 2\cos\left(2\left(\omega + \vartheta\right)\right)\sin^2 i \end{cases} \tag{19}$$

B. Modified equinoctial elements

From Eq. (1) and using the mappings shown in Eq. (15), the magnitude of the thrust-induced acceleration and pitch angle are obtained as shown in Eqs. (20) – (21).

$$\left\| \boldsymbol{a}\left(\boldsymbol{x}_{MEE} \right) \right\| = \frac{\mu q}{sp^2}\sqrt{4q^2\left(k\cos L - h\sin L\right)^2 + \sigma_2\left[q - \frac{s^2\left(1 + f^2 + g^2 + 2f\cos L + 2g\sin L\right)}{\sigma_2} \right]^2} \tag{20}$$

$$\tan\alpha\left(\boldsymbol{x}_{MEE} \right) = \frac{\sqrt{\sigma_2}}{2\left(h\sin L - k\cos L\right)}\left[1 - \frac{s^2\left(1 + f^2 + g^2 + 2f\cos L + 2g\sin L\right)}{q\cdot\sigma_2} \right] \tag{21}$$

The terms s and β in Eqs. (20) – (21) are defined in Eq. (16), whereas q and σ_2 are

$$\begin{cases} q = 1 + f\cos L + g\sin L \\ \sigma_2 = 1 + \left(h^2 + k^2\right)^2 + 2\beta\cos\left(2L\right) + 4hk\sin\left(2L\right) \end{cases} \tag{22}$$

VI. Numerical Test Cases

Several test cases are chosen to assess the validity of the mappings, investigate the behavior of the osculating elements and understand the impact of uncertainties on the mappings. An analytical and numerical sensitivity analysis is performed for the case of the vertical-displacement model, for which both forward and inverse analytical mappings are available. For what concerns the general model with an arbitrary orientation of the NKO plane (which will be referred to as the "arbitrary-orientation model"), key signatures of highly non-Keplerian orbits are then sought. However, these are valid only when the orbit properties are perfectly known. For this reason, a preliminary study is provided which considers the impact of noise on the orbit determination process. This gives a different view of the key signatures with a more practical focus on the orbit determination issue.

For the sake of conciseness, only the most interesting results are shown here. In the following sections, the test cases related to both the vertical-displacement and arbitrary-orientation models are shown and discussed.

A. Vertical-Displacement Model

A Geostationary Earth Orbit (GEO) is chosen as the reference Keplerian orbit. In terms of NKO elements, a GEO is characterized by [18]

$$\text{GEO}: \begin{cases} z = 0 \\ \rho = r_{GEO} = 42{,}164.1696 \text{ km} \\ \varpi = \sqrt{\mu / r_{GEO}^3} \end{cases} \tag{23}$$

Two displaced GEOs are chosen as test cases in this study: a Type 1 NKO and an in-plane Type 3 NKO. Station-keeping regulations currently require a station-keeping box of $0.1 - 0.2$ deg [18]. Therefore, the out-of-plane displacement for the Type 1 NKO is chosen such that the spacecraft hovers just above the GEO station-keeping box. The same displacement is considered in the in-plane case. The NKO elements of the two test cases are then

$$\text{Type 1 NKO}: \begin{cases} z = \pm 35 \text{ km} \\ \rho = r_{GEO}\cos\left(z / r_{GEO}\right) \simeq r_{GEO}, \\ \varpi = \varpi_{GEO} = \sqrt{\mu / r_{GEO}^3} \end{cases} \quad \underset{\text{(in-plane)}}{\text{Type 3 NKO}}: \begin{cases} z = 0 \\ \rho = r_{GEO} \pm 35 \text{ km} \\ \varpi = \varpi_{GEO} = \sqrt{\mu / r_{GEO}^3} \end{cases} \tag{24}$$

1. Forward Maps

Figure 2 shows the Type 1 NKO with $z>0$ as described by Eq. (24), together with its osculating Keplerian orbits, corresponding to the instantaneous orbital elements of the spacecraft if the thrust is nulled. In this case, it is shown how the semi-major axis and eccentricity of the osculating orbits do not change, but the osculating orbit plane rotates around the vertical axis. In fact, Ω is the only osculating KEP that varies with time. All other osculating KEP are constant, as shown in Eq. (7). The spacecraft is always at the apogee of the osculating Keplerian orbits, which then describes the corresponding desired NKO. Therefore, the envelope resulting from the osculating Keplerian orbits after an entire orbit of the NKO is well approximated by a truncated cone, characterized by height H and radii of the bases r_1, r_2 (Eq. (25)).

$$\begin{cases} r_1 = a(1-e)\cos i \\ r_2 = \rho \\ H = |z| + |a(1-e)\sin i| \end{cases} \tag{25}$$

Figure 3 shows an in-plane Type 3 displaced GEO with $\rho = r_{GEO} + 1000$ km, together with its osculating Keplerian orbits. The arrows shown in Fig. 3 point to the perigee of each orbit. In this case, it is shown how the semi-major axis and eccentricity of the osculating orbits do not change, but the osculating argument of pericenter rotates around the vertical axis. In fact, ω is the only osculating KEP that varies with time. All other osculating KEP are constant, as shown in Eq. (7). The spacecraft is always at the perigee of the osculating Keplerian orbits, which again describes the corresponding desired NKO.

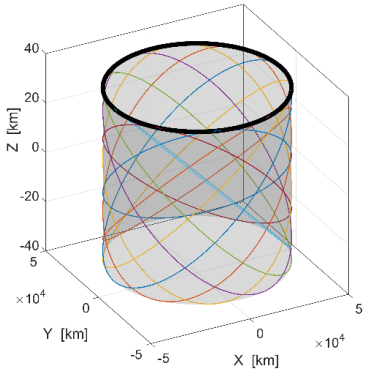

Fig. 2 Type 1 NKO displaced GEO (solid black line) and osculating Keplerian orbits.

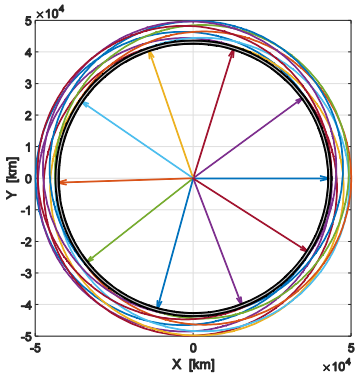

Fig. 3 Type 3 NKO 1000-km in-plane displaced GEO (solid black line) and osculating Keplerian orbits.

To investigate the sensitivity analysis of the forward maps, the relative error of the NKO elements is considered fixed and constant, such that $\varepsilon_z = \varepsilon_\rho = \varepsilon_\varpi = 10^{-3}$. Considering the characteristics of the orbits shown in Eq. (24), the absolute errors on the NKO elements considered for the sensitivity analysis are

$$\text{Type 1 NKO}: \begin{cases} \delta z_1 = \varepsilon_z z_1 \simeq 0.15 \text{ km} \\ \delta\rho_1 = \varepsilon_\rho \rho_1 \simeq 42.2 \text{ km} \\ \delta\varpi_1 = \varepsilon_\varpi \varpi_1 \simeq 0.36 \text{ deg/day} \end{cases}, \quad \text{Type 3 NKO (in-plane)}: \begin{cases} \delta z_3 = \varepsilon_z z_1 \simeq 0.15 \text{ km} \\ \delta\rho_3 = \varepsilon_\rho \rho_3 \simeq 42.2 \text{ km} \\ \delta\varpi_3 = \varepsilon_\varpi \varpi_3 \simeq 0.36 \text{ deg/day} \end{cases} \tag{26}$$

Note that the term δz_3 in Eq. (26) depends on the displacement of the Type 1 NKO. This is made on purpose to have a non-zero error for the out-of-plane displacement.

Figure 4 shows the evolution over one orbit of the osculating in-plane MEE f for the case of the Type 1 NKO. The nominal value and the values due to errors in the NKO elements are shown. The error on the in-plane element f due to uncertainties in the NKO elements is of the same order of magnitude as the uncertainties themselves. The same behavior is noted in the other in-plane modified equinoctial element g. On the other hand, Fig. 5 shows the evolution over one orbit of the out-of-plane MEE h for the case of Type 1 NKO. The nominal value and the values due to errors in the NKO elements are shown. Figure 5 shows that the error on the out-of-plane element h due to uncertainties in the NKO elements is orders of magnitude smaller than the value of the uncertainties. The same behavior is noted in the other out-of-plane modified equinoctial element k. Here, the semi-latus rectum shows a constant error due to uncertainties in the NKO elements of the same order of magnitude as the uncertainties themselves. Lastly, the true longitude exhibits a linearly increasing error due to a 0.1% uncertainty on the orbit angular velocity. After one orbit, the absolute error on the true longitude is therefore 0.36 deg.

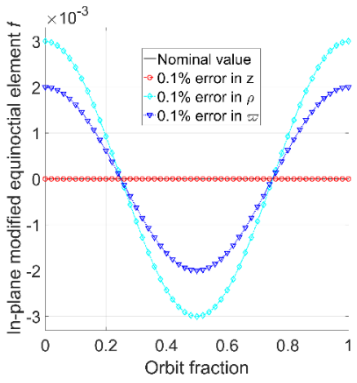

Fig. 4 Evolution of the *f* over one orbit.

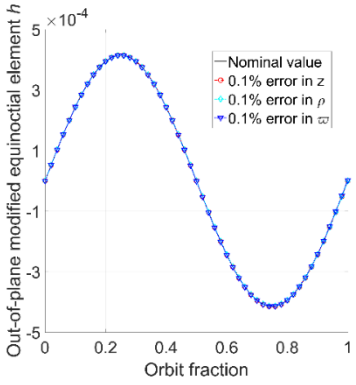

Fig. 5 Evolution of *h* over one orbit.

2. Inverse Maps

The same test cases used to study the forward maps are now considered for the study of the inverse maps. All the results of the mappings have been numerically verified against their nominal values. That is, the osculating orbital elements have been obtained through the forward mappings starting from the nominal NKO elements. Then, the inverse mappings are used to obtain the original NKO elements. The errors between the nominal values of the NKO elements and those obtained after the conversion gives an estimate of the accuracy of both forward and inverse mappings. This results in errors of less than 10^{-9} km for z and ρ, and errors of less than 10^{-12} deg/day for ϖ. This validates the inverse maps.

For the sensitivity analysis, the errors of the osculating KEP and MEE are considered fixed and constant, as follows.

$$\text{KEP}: \begin{cases} \varepsilon_a = 10^{-3} \text{ (relative)} \\ \varepsilon_e = 10^{-3} \text{ (absolute)} \\ \varepsilon_{\{i,\Omega,\omega,\vartheta\}} = 10^{-3} \cdot \pi \end{cases}, \quad \text{MEE}: \begin{cases} \varepsilon_p = 10^{-3} \text{ (relative)} \\ \varepsilon_{\{f,g,h,k\}} = 10^{-3} \text{ (absolute)} \\ \varepsilon_L = 10^{-3} \cdot \pi \end{cases} \tag{27}$$

in which the errors relative to angular quantities are considered as 0.1% of the maximum possible error (π).

The sensitivity analysis demonstrates that the planar elements (i.e. ρ, ϖ) of both mappings are robust to uncertainties in the osculating orbital elements. Both mappings of the out-of-plane displacement z are robust to uncertainties in the in-plane osculating elements. However, the out-of-plane displacement is very sensitive to errors in the out-of-plane osculating elements. This is understandable if the osculating Keplerian orbit has a small inclination and a large semi-major axis ($a \sim r_{GEO}$ in this case).

Figure 6 shows the relative error evolution of the orbit radius ρ over one orbit obtained from the osculating MEE with an error of 0.001 in the in-plane MEE f. Both test cases are shown. It is shown that the relative error on the orbit radius is at most the same order of magnitude as the initial uncertainty itself. Figure 7 shows the evolution of the out-of-plane displacement z over one orbit obtained from the osculating MEE. Both test cases are shown. Both the nominal value and an error of 0.001 in the out-of-plane MEE h are considered. It is shown how a small error in the out-of-plane element can cause a large error in the out-of-plane displacement, as discussed above.

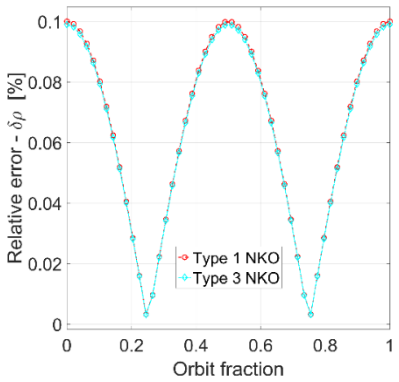

Fig. 6 Relative error in orbit radius in case of an error of 0.001 in *f*.

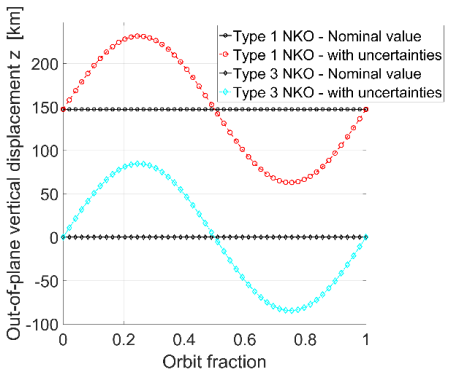

Fig. 7 Out-of-plane displacement. Nominal case and error of 0.001 in *h*.

3. Thrust-induced acceleration

The acceleration, in terms of magnitude and pitch angle, resulting from both Eqs. (17) – (18) and Eqs. (20) – (21) has been validated using two separate checks. In the first check, the values of the magnitude and pitch angle are compared with those given directly by using Eq. (1). The values of both the magnitude and direction of the acceleration have been verified for all test cases considered with both sets of elements. The errors in magnitude and direction of the acceleration are $\|\delta\boldsymbol{a}\| \le 10^{-11}\ \mathrm{mm/s^2}$ and $|\delta\alpha| \le 10^{-12}$ rad, respectively. The second check has been carried out by propagating the equations of motion with the propulsive acceleration given by Eqs. (17) – (18) and Eqs. (20) – (21), respectively. The relative errors in position and velocity vectors between the initial state and the state after one orbital period are used to validate the acceleration. A variable order Adam-Bashford-Moulton PECE solver (as implemented in MATLAB *ode113*) with relative and absolute tolerances equal to 10^{-10} and 10^{-12}, respectively, has been used for the propagation of the equations of motion. The relative errors in the final position and velocity are $\|\delta\boldsymbol{r}\|/\|\boldsymbol{r}\| \simeq \|\delta\boldsymbol{v}\|/\|\boldsymbol{v}\| \le 10^{-9}$.

Lastly, the accelerations required for the test cases have magnitudes $\|\boldsymbol{a}\| = \{0.19, 0.56\}\ \mathrm{mm/s^2}$ for Type 1 and Type 3 NKOs, respectively. Considering a 1000-kg spacecraft, such accelerations can be converted into maximum required thrusts $T_{max} = \{0.19, 0.56\}$ N that are feasible values for near-term low-thrust technology [19].

4. Summary

The use of classical Keplerian elements to describe the osculating orbits is impractical for the forward map mainly because of the piecewise formulation of most of the elements. On the other hand, KEP are good candidates

to be used for the inverse map because of their easy formulation and robustness to uncertainties. The use of modified equinoctial elements to describe the osculating orbits is also a good choice due to their easy formulation and robustness to uncertainties. Moreover, for the same reasons, MEE are good candidates to be used for the inverse map as well. In conclusion, the use of MEE guarantees an easy and robust formulation for both forward and inverse mappings in the case of the vertical-displacement model, with the NKO orbital plane parallel to the equatorial plane. Lastly, the analytical formulations of the thrust-induced acceleration starting from both KEP and MEE have been demonstrated to be valid.

A summary of the advantages and drawbacks of the mappings for both the direct and inverse problems is shown in Tables 1 and 2, respectively, for the two sets of osculating elements considered.

Table 1 Map from NKO to osculating orbital elements. Summary of advantages and drawbacks.

	KEP	MEE
Advantages	• Easy to understand • Only one element is time dependent	• Easy formulation (no piecewise cases) • Robust to uncertainties • Robust to the switch apocenter/pericenter • No singularities • 5 elements are time dependent
Drawbacks	• Piecewise formulation • Very sensitive to uncertainties • Issues around $z = 0$ • Singularity: $\Omega = 0$ if $z = 0$ • Very sensitive to the switch apocenter/pericenter	

Table 2 Map from Osculating orbital elements to NKO. Summary of advantages and drawbacks.

	KEP	MEE
Advantages	• Easy to understand • Easy formulation • Robust to uncertainties	• Easy formulation • Robust to uncertainties on in-plane elements
Drawbacks	• Out-of-plane displacement very sensitive to uncertainties on inclination	• Out-of-plane displacement very sensitive to uncertainties on out-of-plane elements

B. Arbitrary-Orientation Model

Three scenarios have been tested to both verify the validity of the arbitrary-orientation forward mappings and investigate the behavior of the osculating orbital elements. The three test cases have been chosen to represent

feasible mission scenarios in the near future. For this reason, only small-displacement NKOs are considered which can be generated with near-term technology.

The first scenario consists of a 35-km out-of-plane (Type 1) and in-plane (Type 3) displaced GEO, as described in the case of the vertical-displacement model. The second scenario is a 5-km out-of-plane (Type 1) and in-plane (Type 3) displaced global positioning system (GPS) orbit. In this scenario, the spacecraft hovers above/below or inside/outside the GPS spacecraft for visual inspection. Moreover, a distance of 5 km can be considered within the range for proximity operations [20]. The third and last scenario considered is a 1-km out-of-plane (Type 1) and in-plane (Type 3) displaced Sun-synchronous orbit (SSO). As for the previous scenario, a 1-km range can be used for visual inspection of the SSO satellite and is within the range for proximity operations. In terms of NKO elements, the characteristics of the GEO orbit are defined in Eq. (23) together with $j = \xi = 0$. The GPS and SSO orbits are characterized, in terms of NKO elements, by

$$\text{GPS}: \begin{cases} z = 0 \\ \rho = r_{GPS} = 26{,}560.9478 \text{ km} \\ \varpi = \sqrt{\mu / r_{GPS}^3} \\ j = 55.2885 \text{ deg} \\ \xi = 77.7881 \text{ deg} \end{cases}, \quad \text{SSO}: \begin{cases} z = 0 \\ \rho = r_{SSO} = 7378.16 \text{ km} \\ \varpi = \sqrt{\mu / r_{SSO}^3} \\ j = 99.4845 \text{ deg} \\ \xi = 0 \end{cases} \tag{28}$$

1. Signatures

These test cases have been used to seek key characteristics of signatures that can provide a simple and reliable indication that a spacecraft is being forced along a highly non-Keplerian orbit. Both KEP and MEE are characterized by four elements that can be used to identify a NKO. Therefore, assuming perfect knowledge of the NKO geometry, the elements that show a peculiar trend are shown in Eq. (29), in which $\tilde{\tau}$ is the semi-amplitude of the cosine wave related to the element τ and φ is a generic phase.

$$\text{KEP}: \begin{cases} i(t) \simeq \tilde{i} \cos(\varpi t + \varphi) & \text{if } z \neq 0 \wedge j \neq 0 \\ \Omega(t) = \Omega_0 + \varpi t & \text{if } z \neq 0 \wedge j = 0 \\ \Omega(t) \simeq \tilde{\Omega} \cos(\varpi t + \varphi) & \text{if } z \neq 0 \wedge j \neq 0, \\ \omega(t) = \omega_0 + \varpi t & \text{if } z = 0 \vee j \neq 0 \\ \vartheta(t) = \vartheta_0 \end{cases} \quad \text{MEE}: \begin{cases} f(t) \simeq \tilde{f} \cos(\varpi t + \varphi) \\ g(t) \simeq \tilde{g} \cos(\varpi t + \varphi) \\ h(t) \simeq \tilde{h} \cos(\varpi t + \varphi) & \text{if } z \neq 0 \\ k(t) \simeq \tilde{k} \cos(\varpi t + \varphi) & \text{if } z \neq 0 \end{cases} \tag{29}$$

2. Impact of noise

The impact of noise on the NKO elements is considered here to investigate the signatures of NKOs in the presence of noise on orbit determination. As such, a set of practical preliminary guidelines can be drawn to

understand, from observation data, whether a spacecraft is being forced on a highly non-Keplerian orbit. The same scenarios used to study the signatures have been considered. However, only the Type 1 NKOs with a positive displacement are considered.

Three values for the noise have been considered in this study, consisting of upper/lower boundaries and a value inside this range. The upper boundary considers tracking instrumental errors, whereas noise due to statistical filtering is considered as the lower boundary. The three sets of errors considered here are the following [21].

$$\begin{aligned}
&\text{Case 1}\\
&\text{(upper bound)}
\end{aligned}: \begin{cases} \|\Delta \boldsymbol{r}\| = 24 \text{ m} \\ |\Delta i| = 0.01 \text{ deg} \\ |\Delta\Omega| = \begin{cases} 180 \text{ deg} & \text{if GEO} \\ 0.01 \text{ deg} & \text{otherwise} \end{cases} \end{cases}, \quad \text{Case 2}: \begin{cases} \|\Delta \boldsymbol{r}\| = 2.4 \text{ m} \\ |\Delta i| = 0.001 \text{ deg} \\ |\Delta\Omega| = \begin{cases} 180 \text{ deg} & \text{if GEO} \\ 0.001 \text{ deg} & \text{otherwise} \end{cases} \end{cases} \tag{30}$$

$$\begin{aligned}
&\text{Case 3}\\
&\text{(lower bound)}
\end{aligned}: \begin{cases} \text{GEO:} \begin{cases} \|\Delta \boldsymbol{r}\| = 0.1 \text{ m} \\ |\Delta i| = 10^{-3} \text{ deg} \\ |\Delta\Omega| = 2\times 10^{-3} \text{ deg} \end{cases}, \quad \text{GPS/SSO:} \begin{cases} \|\Delta \boldsymbol{r}\| = 1 \text{ m} \\ |\Delta i| = 10^{-4} \text{ deg} \\ |\Delta\Omega| = 10^{-4} \text{ deg} \end{cases} \end{cases}$$

The errors $\{\|\Delta \boldsymbol{r}\|, |\Delta i|, |\Delta\Omega|\}$ are used to estimate the noise to be considered for the NKO elements. A Monte Carlo analysis has been carried out with 500 samples of NKO elements in a normal distribution. The mean values considered are the nominal values of the NKO elements $\{z_0, \rho_0, j_0, \xi_0\}$, whereas the standard deviations are $\{\|\Delta \boldsymbol{r}\| \sin(z_0/\rho_0), \sqrt{3}\|\Delta \boldsymbol{r}\|, |\Delta i|, |\Delta\Omega|\}$, respectively. The value of the angular velocity is simply given by $\varpi = \sqrt{\mu/\rho^3}$, in which ρ is the NKO orbit radius with noise.

Figures 8 and 9 both show GEO and Type 1 NKOs in the presence of noise from Eq. (30) for cases 1 and 2, respectively. Both figures have been generated using the Cartesian position vectors resulting from the osculating KEP obtained through the forward map from NKO elements with noise. The figures show that the Keplerian GEO and the NKO are clearly distinguishable for the noise related to Case 2. On the contrary, the same is not true for the three-dimensional orbits of both the GPS and SSO cases. That is, in the GPS and SSO cases, one cannot determine if the orbit is Keplerian or highly non-Keplerian. The thrust-induced acceleration and the evolution of the MEE k among all scenarios and noise levels are shown in [21] and not reported here for the sake of conciseness.

3. Summary

In Table 3, the impact of noise on the mappings is summarized. Those signatures that, despite the noise, can provide a clear and reliable indication that a spacecraft is being forced along a highly non-Keplerian orbit are

highlighted for each case study under consideration. It is important to note that, in this case, both sets of elements (KEP and MEE) are important in the understanding of the NKO signatures in the presence of noise.

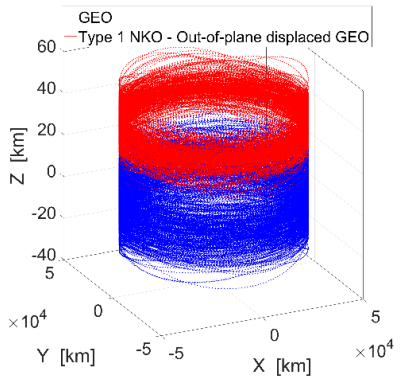

Fig. 8 GEO and NKO. Noise level case 1.

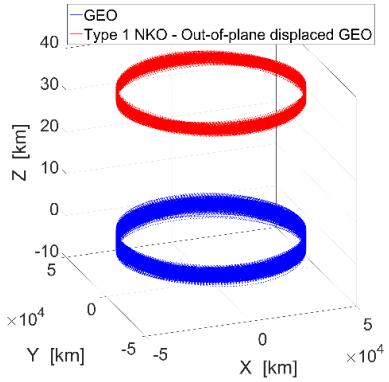

Fig. 9 GEO and NKO. Noise level case 2.

Table 3 Summary of the impact of noise on the NKO signatures.

	Signatures	Issues
GEO	GEO and NKO are clearly defined from the following (Cases 2-3 only): • 3D orbits • Osculating inclination • $\|\boldsymbol{a}\|$ (vertical-displacement analytical approach)	• Case 1 is too noisy • From $\{\Omega, \omega, \vartheta\}$ and all MEE, GEO and NKO are not clearly defined
GPS SSO	GPS/SSO and NKO are clearly defined from the following (Cases 2-3 only): • Elements $\{i, \Omega, h, k\}$ • $\|\boldsymbol{a}\|$ (vertical-displacement analytical approach)	• Case 1 is too noisy • From $\{\omega, \vartheta\}$, GPS/SSO and NKO are not clearly defined • The magnitude of the in-plane MEE is too small • GPS/SSO and NKO are not clearly defined from the 3D orbits • $\|\boldsymbol{a}\|$ can be used only if i and Ω are known.

VII. Conclusions

This note has presented a mapping between highly non-Keplerian orbit (NKO) geometry and classical orbital elements for both the direct and inverse problem. Two sets of elements have been discussed which are the classical Keplerian elements (KEP) and the modified equinoctial elements (MEE). The forward map has been derived in closed, analytical form for a generic NKO, which is the so-called arbitrary-orientation model. Furthermore, a

specific case, in which the NKO orbital plane is parallel to the $\hat{\boldsymbol{X}}-\hat{\boldsymbol{Y}}$ plane (the so-called vertical-displacement model), has been studied in detail and both direct and inverse mappings have been derived in closed, analytical form. For the vertical-displacement model, it has been shown that the main drawback of using the KEP is due to the piecewise formulation required for a forward mapping. The MEE, on the other hand, provide both a simple formulation and have low sensitivity to uncertainties in both the forward and inverse mappings. For the arbitrary-orientation model, it has been shown that both KEP and MEE are characterized by piecewise formulations. Three test cases have been chosen that show a broad range of applicability of the maps. Using the same test cases, noise has been added to the initial NKO elements to assess the impact on estimates of the classical orbital elements. It has been demonstrated that, despite the noise, signatures exist that can provide a clear and reliable indication that a spacecraft is being forced along an NKO. Both KEP and MEE have equal advantages and drawbacks in the case of the arbitrary-orientation forward map in the presence of noise. Therefore, in order to clearly distinguish a Keplerian orbit from a NKO using their orbital elements, it is important to look at: a) three-dimensional orbit; b) osculating i and Ω; c) osculating out-of-plane MEE h and k; and d) magnitude of the thrust-induced acceleration. This can provide an initial understanding for future, detailed analysis of optimal estimation using statistical filtering.

Acknowledgments

This material is based upon work supported by the Air Force Office of Scientific Research under award number FA9550-16-1-0219. CM was supported by a Royal Society Wolfson Research Merit Award.

References

[1] McKay, R., Macdonald, M., Biggs, J. and McInnes, C., "Survey of Highly Non-Keplerian Orbits with Low-Thrust Propulsion," *Journal of Guidance, Control, and Dynamics*, Vol. 34, No. 3, 2011, pp. 645-666.
doi: 10.2514/1.52133

[2] McInnes, C. R., "The Existence and Stability of Families of Displacement Two-Body Orbits," *Celestial Mechanics and Dynamical Astronomy*, Vol. 67, No. 2, 1997, pp. 167-180.
doi: 10.1023/a:1008280609889

[3] McInnes, C. R., "Dynamics, Stability, and Control of Displaced Non-Keplerian Orbits," *Journal of Guidance, Control, and Dynamics*, Vol. 21, No. 5, 1998, pp. 799-805.

doi: 10.2514/2.4309

[4] Heiligers, J., McInnes, C. R., Biggs, J. D. and Ceriotti, M., "Displaced geostationary orbits using hybrid low-thrust propulsion," *Acta Astronautica*, Vol. 71, 2012, pp. 51-67.

doi: 10.1016/j.actaastro.2011.08.012

[5] Xu, M. and Xu, S., "Nonlinear dynamical analysis for displaced orbits above a planet," *Celestial Mechanics and Dynamical Astronomy*, Vol. 102, No. 4, 2008, pp. 327-353.

doi: 10.1007/s10569-008-9171-4

[6] McInnes, C. R., "Displaced non-Keplerian orbits using impulsive thrust," *Celestial Mechanics and Dynamical Astronomy*, Vol. 110, No. 3, 2011, pp. 199-215.

doi: 10.1007/s10569-011-9351-5

[7] Macdonald, M., McKay, R. J., Vasile, M., Bosquillon De Frescheville, F., Biggs, J. and McInnes, C., "Low-Thrust-Enabled Highly-Non-Keplerian Orbits in Support of Future Mars Exploration," *Journal of Guidance, Control, and Dynamics*, Vol. 34, No. 5, 2011, pp. 1396-1411.

doi: 10.2514/1.52602

[8] Ceriotti, M., Diedrich, B. L. and McInnes, C. R., "Novel mission concepts for polar coverage: An overview of recent developments and possible future applications," *Acta Astronautica*, Vol. 80, 2012, pp. 89-104.

doi: 10.1016/j.actaastro.2012.04.043

[9] Mengali, G. and Quarta, A. A., "Non-Keplerian orbits for electric sails," *Celestial Mechanics and Dynamical Astronomy*, Vol. 105, No. 1, 2009, pp. 179-195.

doi: 10.1007/s10569-009-9200-y

[10] Spilker, T. R., "Saturn Ring Observer," *Acta Astronautica*, Vol. 52, No. 2–6, 2003, pp. 259-265.

doi: 10.1016/S0094-5765(02)00165-0

[11] McInnes, C. R., "Space-based geoengineering: Challenges and requirements," *Proceedings of the Institution of Mechanical Engineers, Part C: Journal of Mechanical Engineering Science*, Vol. 224, No. 3, 2010, pp. 571-580.

doi: 10.1243/09544062jmes1439

[12] Jin, Z. and Tianshu, W., "Coupled Attitude-Orbit Control of Flexible Solar Sail for Displaced Solar Orbit," *Journal of Spacecraft and Rockets*, Vol. 50, No. 3, 2013, pp. 675-685.

doi: 10.2514/1.A32369

[13] Huo, M., Liao, H., Liu, Y. and Qi, N., "The Coupled Orbit-Attitude Dynamics and Control of Electric Sail in Displaced Solar Orbits," *International Journal of Aerospace Engineering*, Vol. 2017, 2017.

doi: 10.1155/2017/3812397

[14] Gong, S., Li, J. and BaoYin, H., "Formation flying solar-sail gravity tractors in displaced orbit for towing near-Earth asteroids," *Celestial Mechanics and Dynamical Astronomy*, Vol. 105, No. 1, 2009, pp. 159.

doi: 10.1007/s10569-009-9211-8

[15] Curtis, H., *Orbital Mechanics for Engineering Students*, Second Edition, Elsevier Science, 2009, pp. 209 - 212.

[16] Walker, M. J. H., Ireland, B. and Owens, J., "A set of modified equinoctial orbit elements," *Celestial Mechanics*, Vol. 36, No. 4, 1985, pp. 409-419.

doi: 10.1007/bf01227493

[17] Betts, J. T., *Practical Methods for Optimal Control and Estimation Using Nonlinear Programming (Second Edition)*, Soc. for Industrial and Applied Mathematics, Philadelphia, PA, USA, 2010, pp. 265-267.

[18] Heiligers, J., Ceriotti, M., McInnes, C. R. and Biggs, J. D., "Displaced Geostationary Orbit Design Using Hybrid Sail Propulsion," *Journal of Guidance, Control, and Dynamics*, Vol. 34, No. 6, 2011, pp. 1852-1866.

doi: 10.2514/1.53807

[19] Gates, M., Stich, S., McDonald, M., Muirhead, B., Mazanek, D., Abell, P. and Lopez, P., "The Asteroid Redirect Mission and sustainable human exploration," *Acta Astronautica*, Vol. 111, 2015, pp. 29-36.

doi: 10.1016/j.actaastro.2015.01.025

[20] Howard, R. T., Bryan, T. C., Brewster, L. L. and Lee, J. E., "Proximity operations and docking sensor development," *2009 IEEE Aerospace Conference*, IEEE Paper 1287, Big Sky, MT, USA, 2009.

[21] Peloni, A., McInnes, C. R. and Ceriotti, M., "Osculating Keplerian Elements for Highly Non-Keplerian Orbits," *27th AAS/AIAA Space Flight Mechanics Meeting*, AAS Paper 17-278, San Antonio, TX, USA, 2017.